Supporting Information

Unravelling the role of benzoquinone intercalators on the aqueous zinc-ion storage performance toward vanadium pentoxide cathode

Yuanhao Xia, Qin Cao, Yan Wang, Xinlei Wang*, Jie Zhou*,

Experimental Section

Materials

Vanadium pentoxide (V_2O_5) and N-methylpyrrolidone (NMP) were purchased from Shanghai Aladdin Biochemical Technology Co. Ltd. Benzoquinone (BQ) was purchased from Shanghai Adama Beta Chemical Reagent Co. Ltd. Tetrafluoro-benzoquinone (BQ4F) was purchased from Shanghai Aladdin Biochemical Technology Co. Ltd. Tetrabromo-benzoquinone (BQ4Br) was purchased from Shanghai Yuanye Biotechnology Co. Ltd. Glass fiber membrane (GF/D grade) was provided by Whatman company. Zinc foil (diameter: 15 mm, thickness: 0.3 mm) was purchased from Dongguan Keloude Experimental Materials Technology Co. Ltd. Titanium foil (diameter: 15 mm, thickness: 0.1 mm) was purchased from Guangzhou Haiyuan Metal Products Co. Ltd. Conductive carbon black (Super P Li) was purchased from Guangdong Candlelight New Energy Technology Co. Ltd. Polyvinylidene fluoride (PVDF) was purchased from Wuyu Chemical Industry Co. Ltd. Zinc trifluoromethylsulfonate ($Zn(CF_3SO_3)_2$) was purchased from Shanghai McLean Biochemical Technology Co. Ltd.

Synthesis of V_2O_5-BQ, V_2O_5-BQ4F and V_2O_5-BQ4Br

The V_2O_5-BQ (V_2O_5-BQ4F or V_2O_5-BQ4Br) was synthesized by one-step solvothermal method. 0.002 mol of commercial V_2O_5 and 0.0004 mol of benzoquinone (BQ4F or BQ4Br) were added into 35 ml of deionized water. This suspension was ultrasonic treated for 0.5 h, then sealed in a 50 mL autoclave and kept for 24 h at 160 °C. The product is collected by centrifugal precipitation and washed by deionized water and dichloromethane for several times, finally dried at 80 °C for 12 hours. Following the same conditions, s-V_2O_5 is prepared without adding any benzoquinones.

Characterizations

The crystal structure of the sample was obtained by the radiation X-ray diffractometer (XRD, Japan Science, SmartLab3), and the Fourier infrared spectrum (FTIR) came from the infrared spectrometer (ThermoFisher Nicolet iS-10). Scanning electron microscopy (SEM) and energy dispersive X-ray spectroscopy (EDS) mapping images of the samples were obtained by J Hitachi S-4800 instrument equipped with an EDS (AMETEK) analyzer at an accelerated voltage of 3 kV. X-ray photoelectron spectroscopy (XPS) analysis was performed on the Thermo ESCALAB 250 X-ray photoelectron spectrometer. Electron paramagnetic resonance (EPR) spectroscopy was performed using an EPR (BRUKE EMXPLUS) with a central field of 3600 G and a scanning width of 100G. Nitrogen (N_2) adsorption-desorption curves were measured by a 3Flex three-station universal gas adsorbent (Micromeritics, USA). Thermogravimetric (TG) curves were measured from 50 °C to 800 °C in N_2 atmosphere by TGA/SDTA851E (Mettler Toledo). The Raman spectrum is measured by a Horiba

Scientific LabRAM HR Evolution equipped with a 633 nm He Ne laser. The pore volume and specific surface area were measured by Brunauer-Emmet Teller (BET) surface analyzer (Micromeritics, ASAP 2020). All cyclic voltammetric tests (CV) and electrochemical impedance spectroscopy (EIS)were obtained using CHI760E electrochemical workstation (Chenhua, Shanghai, China). EIS was performed with an AC amplitude voltage of 5 mV in the frequency range of 0.01 Hz~100 kHz. The constant current charge/discharge (GCD) test with voltage range of 0.1V to 1.6 V was conducted on LAND CT2001A (5 V/5 mA).

Battery fabrication

All samples (V_2O_5-BQ, V_2O_5-BQ4F and V_2O_5-BQ4Br) are mixed with Super P Li and PVDF at the ratio of 6:3:1, then NMP is added and fully milled, the resulting slurry is coated on titanium foil, and dried in vacuum at 80 °C for 12 h. The average mass loading is kept in the range of 1.4-1.8 mg cm^{-2}. The CR2032 button battery is used, and the assembly process is in air atmosphere (Zinc foil as anode; glass fiber as separator), with 3 M $Zn(CF_3SO_3)_2$ as aqueous electrolyte. All fabricated batteries were stood at room temperature for 12 h before the electrochemical test.

Density functional theory (DFT) calculations

Theoretical simulation and calculation were based on DFT with the B3LYP/6-31G (d,p) basis set. The solvation effect using implicit solvation model (SMD) for a precise simulation of the experimental conditions in aqueous solution is also considered in the optimization. After the molecules were optimized and calculated by DFT, the files of molecular calculation were further used to calculate electrostatic potential (ESP) by a

software of GaussView 5.0. Molecular surface electrostatic potential was mapped by a software of VMD. Van der Waals surface is defined by electron density level of 0.001 e Bohr-3.

We have employed the Vienna Ab Initio Package (VASP)[1,2] to perform all density functional theory (DFT) calculations within the generalized gradient approximation (GGA) using the Perdew-Burke-Ernzerhof (BQE)[3] formulation. We have chosen the projected augmented wave (PAW) potentials[4,5] to describe the ionic cores and take valence electrons into account using a plane wave basis set with a kinetic energy cutoff of 450 eV. Partial occupancies of the Kohn-Sham orbitals were allowed using the Gaussian smearing method and a width of 0.2 eV. The electronic energy was considered self-consistent when the energy change was smaller than 10^{-5} eV. A geometry optimization was considered convergent when the energy change was smaller than 0.02 eV Å^{-1}. The Brillouin zone was integrated with a Monkhorst-Pack 2×2×3 k-point grid for this calculation. The weak interaction was described by DFT+D3 method using empirical correction in Grimme's scheme[6, 7].
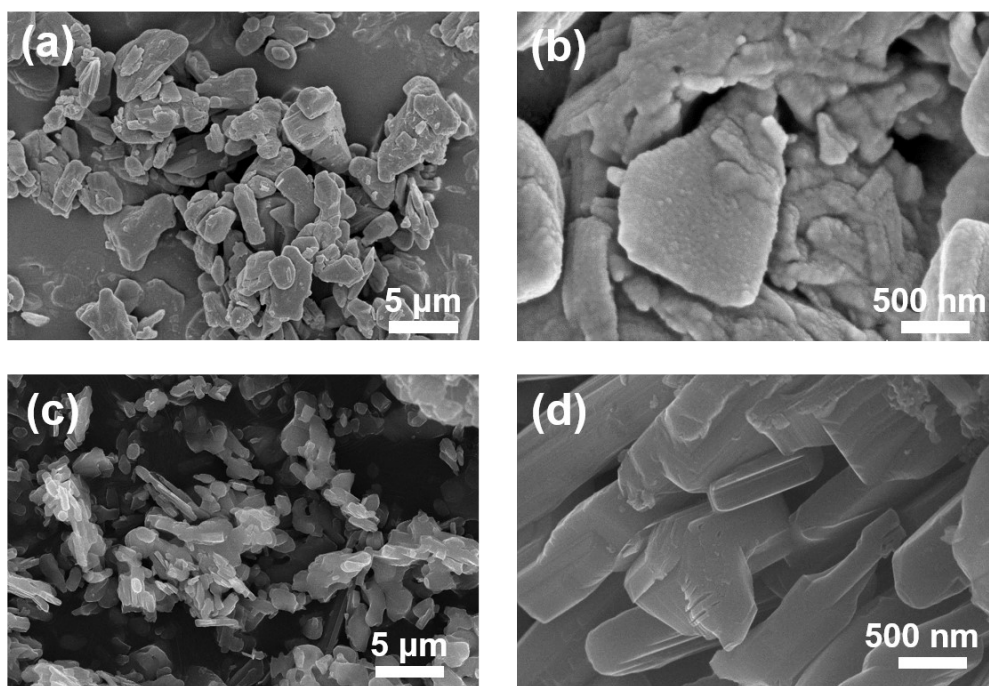
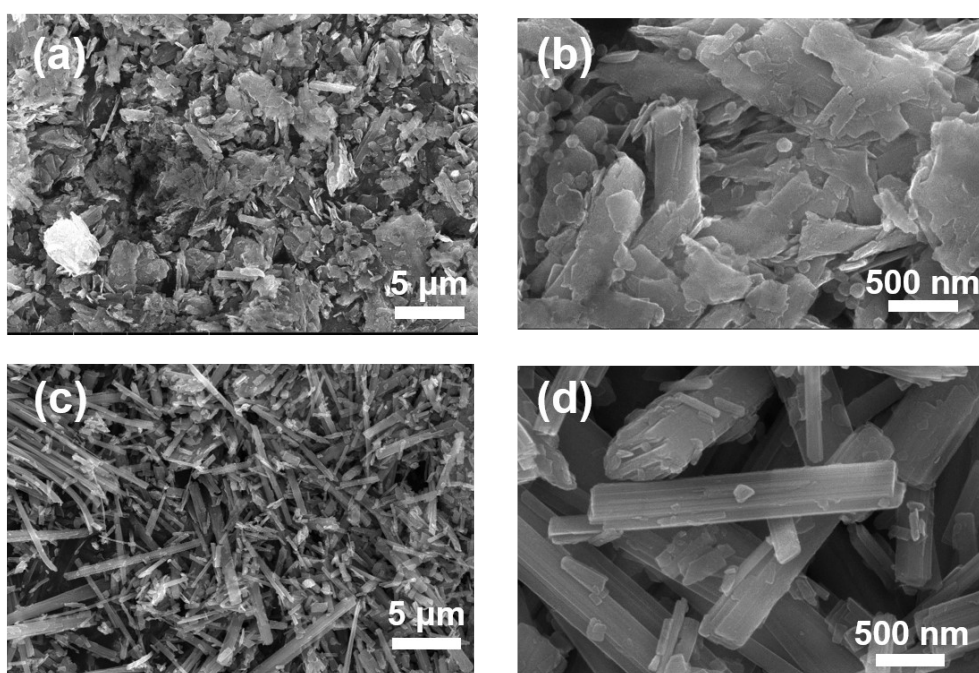**Fig. S1** SEM images of (a, b) s-V_2O_5 and (c, d) commercial V_2O_5.

Fig. S2 SEM images of (a, b) V_2O_5-BQ and (c, d) V_2O_5-BQ4F.
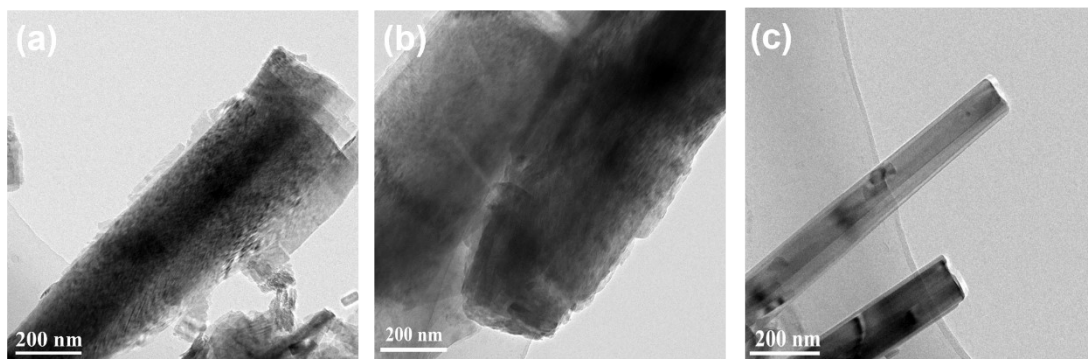
Fig. S3 HRTEM images of (a) V$_2$O$_5$-BQ, (b) V$_2$O$_5$-BQ4Br and (c) V$_2$O$_5$-BQ4F.
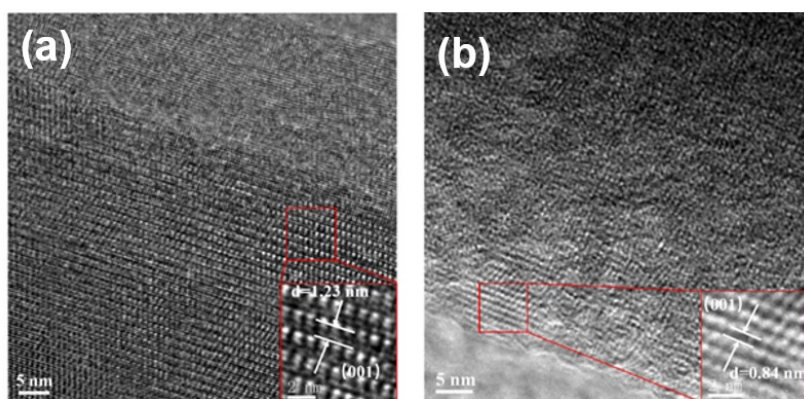

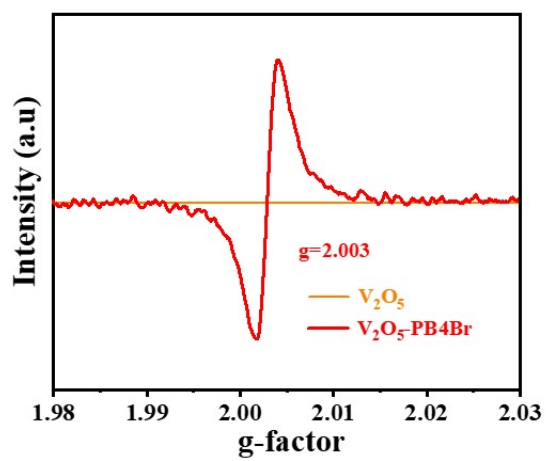**Fig. S4** HRTEM image of lattice line for (a) V$_2$O$_5$-BQ and (b) V$_2$O$_5$-BQ4F.

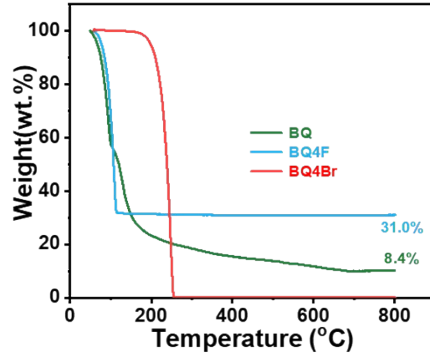**Fig. S5** EFP spectrum of V$_2$O$_5$-BQ4Br.

Fig. S6 TGA curves of BQ, BQ4F and BQ4Br.
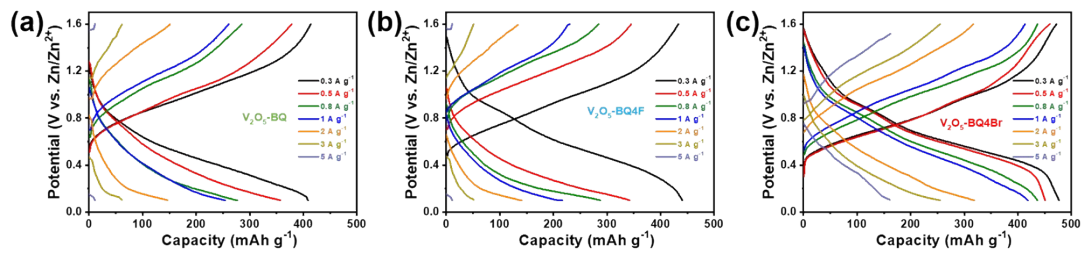

Fig. S7 The GCD curves of (a) V_2O_5-BQ, (b) V_2O_5-BQ4F, and (c) V_2O_5-BQ4Br from 0.3 to 5 A g^{-1}.
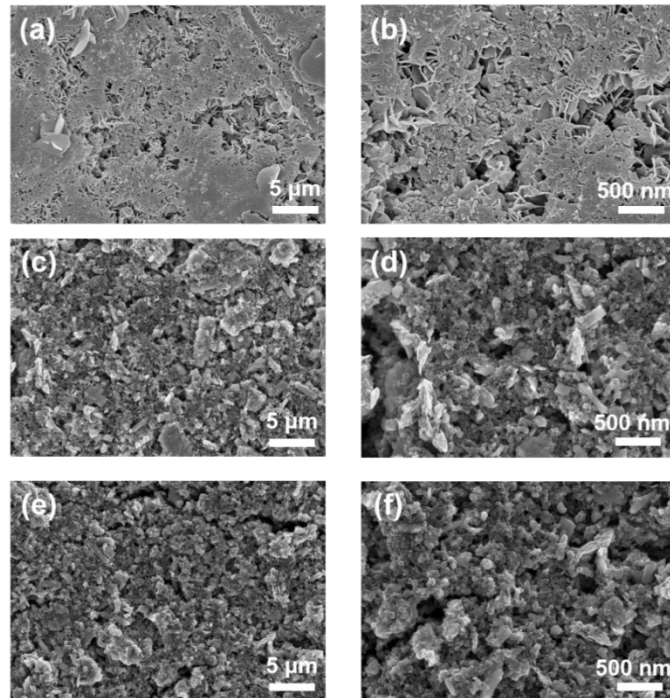

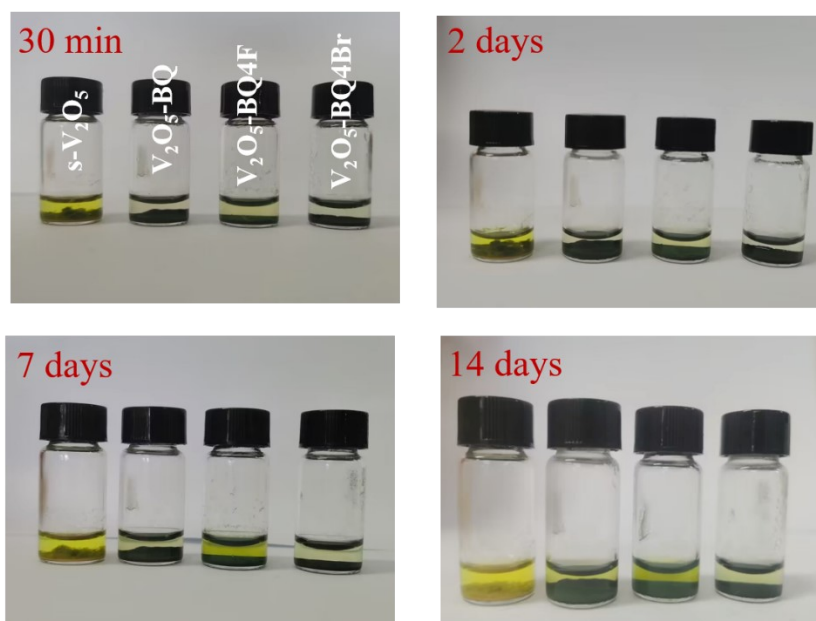**Fig. S8** SEM images of (a, b) V_2O_5-BQ, (c, d) V_2O_5-BQ4F and (e, f) V_2O_5-BQ4Br cathodes after cycles at 3 A g^{-1}.

Fig. S9 Immersion experiment of s-V$_2$O$_5$, V$_2$O$_5$-BQ, V$_2$O$_5$-BQ4F and V$_2$O$_5$-BQ4Br in 3 M Zn(CF$_3$SO$_3$)$_2$.

Table. S1 Comparison of electrochemical properties of novel matter-intercalated V$_2$O$_5$ cathode materials for ZIBs.

Material	Electrolyte	Capacity (Current density)	Capacity retention @current density (Cycle number)	Reference
V$_2$O$_5$	3 M Zn(CF$_3$SO$_3$)$_2$	238 mAh g^{-1} (0.05 A g^{-1})	80%@2 A g^{-1} （2000 cycles）	S8
PANI100– V$_2$O$_5$	3 M Zn(CF$_3$SO$_3$)$_2$	360 mAh g^{-1} (0.5 A g^{-1})	75.6%@5 A g^{-1} （2000 cycles）	S9
VOH-PPy (PSA)	3 M Zn(CF$_3$SO$_3$)$_2$	422 mAh g^{-1} (0.1 A g^{-1})	53.9%@10 A g^{-1} （5000 cycles）	S10
(1, 2, 3-BQ)-VO	3 M Zn(CF$_3$SO$_3$)$_2$	446 mAh g^{-1} (0.2 A g^{-1})	85.4%@5 A g^{-1} （1800 cycles）	S11
PEDOT/V$_2$O$_5$	3 M Zn(CF$_3$SO$_3$)$_2$	247 mAh g^{-1} (0.2 A g^{-1})	88%@10 A g^{-1} （700 cycles）	S12
V2O5@PANI	3 M Zn(CF$_3$SO$_3$)$_2$	361 mAh g^{-1} (0.1 A g^{-1})	93.8%@5 A g^{-1} （1000 cycles）	S13

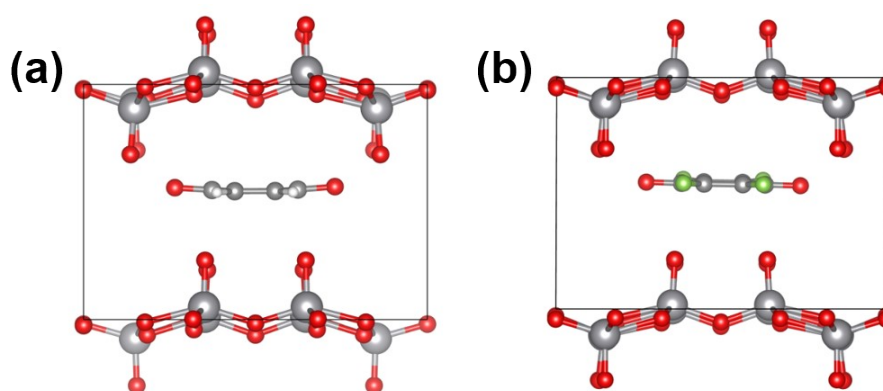|				
PVO@C	3 M Zn(CF$_3$SO$_3$)$_2$	385.3 mAh g^{-1} (0.13 A g^{-1})	86.7%@10 A g^{-1} （5000 cycles）	S14
V$_2$O$_5$-DETA	3 M Zn(CF$_3$SO$_3$)$_2$	180 mAh g^{-1} (0.5 A g^{-1})	92.4%@4 A g^{-1} （1400 cycles）	S15
V$_2$O$_5$-BQ4Br	3 M Zn(CF$_3$SO$_3$)$_2$	477 mAh g^{-1} (0.3 A g^{-1})	75.1%@3 A g^{-1} （5000 cycles）	This work

Fig. S10 Simulated models for binding energies of V$_2$O$_5$ intercalated by (a) BQ and (b) BQ4F.

Table. S2 Calculation process of binding energy of V$_2$O$_5$-BQ, V$_2$O$_5$-BQ4F and V$_2$O$_5$-BQ4Br.

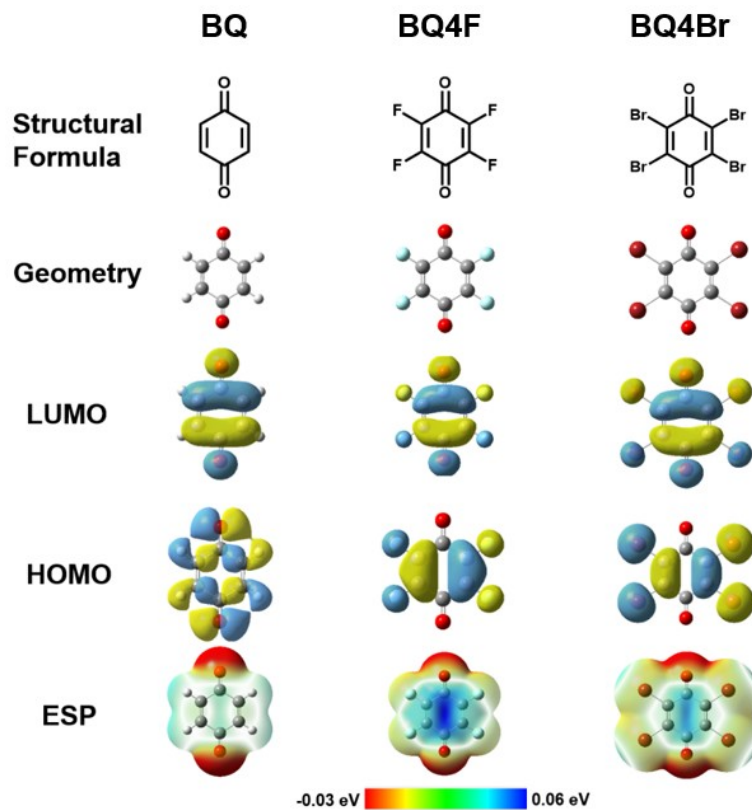|	E_{tot}/eV	E_A/eV	E_B/eV	E_b/eV
V$_2$O$_5$-BQ	-436.24965	-80.704361	-354.7149	-0.830389
V$_2$O$_5$-BQ4F	-436.45547	-80.941105	-354.69973	-0.814635
V$_2$O$_5$-BQ4Br	-428.69888	-72.087293	-354.72959	-1.881997

Fig. S11 DFT-optimized geometries, LUMOs, HOMOs and ESP profiles of BQ, BQ4F and BQ4Br.
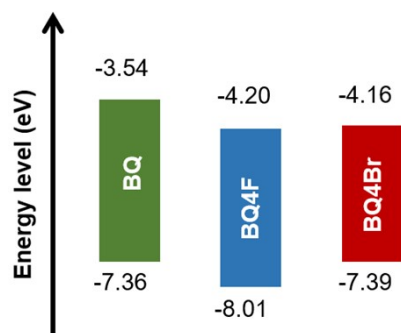

Fig. S12 Energy levels of BQ, BQ4F and BQ4Br.
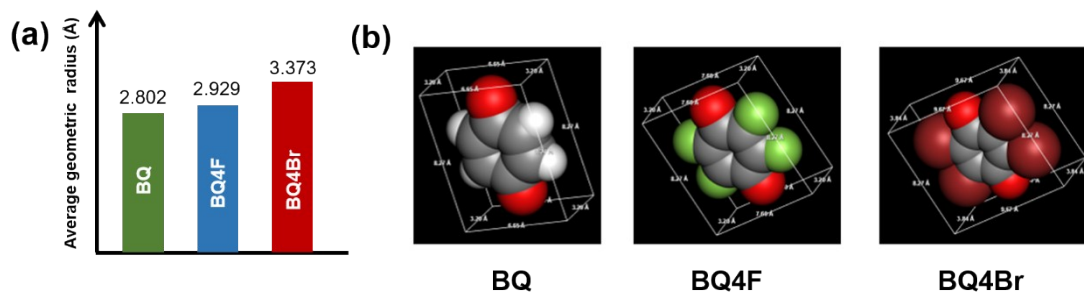

Fig. S13 (a) Calculated average geometric radius and (b) molecular size model of BQ, BQ4F and BQ4Br.
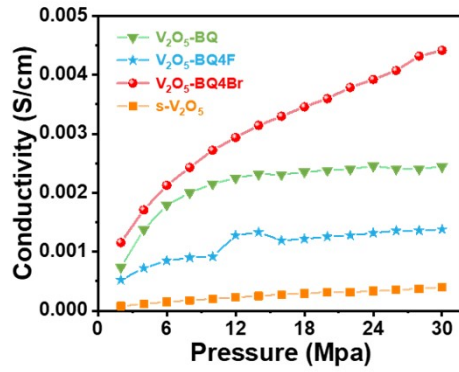
Fig. S14 Electronic conductivity of V_2O_5-BQ, V_2O_5-BQ4F, and V_2O_5-BQ4Br samples.
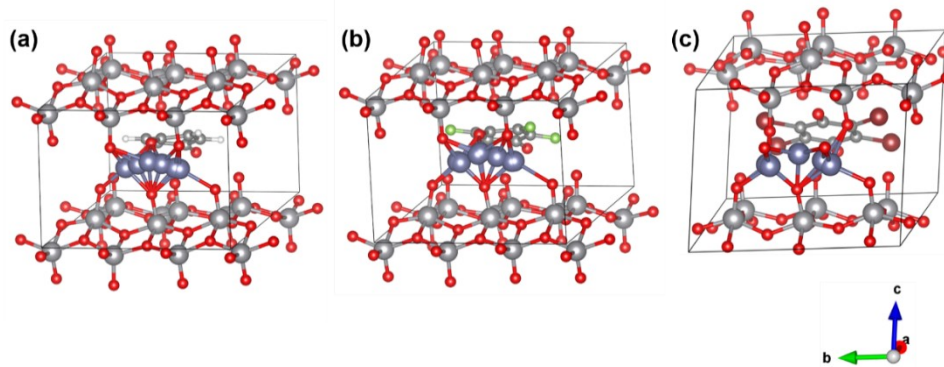

Fig. S15 Simulation of Zn^{2+} migration pathways in (a) V_2O_5-BQ, (b) V_2O_5-BQ4F, and (c) V_2O_5-BQ4Br lattices.

Table. S3 Detailed migration energy barrier of Zn^{2+} in V_2O_5-BQ4Br model.

position	Etot/eV	Energy barriers/eV
1	-431.9887	0
2	-431.9074	0.0813
3	-431.6274	0.3613
4	-431.7826	0.2061
5	-431.7486	0.2401
6	-432.0518	-0.0631
7	-432.2453	-0.2566

Table. S4 Detailed migration energy barrier of Zn^{2+} in V_2O_5-BQ model.

position	Etot/eV	Energy barriers/eV
1	-439.758	0
2	-439.6926	0.0654
3	-439.371	0.387
4	-439.653	0.105
5	-439.4056	0.3524
6	-439.6417	0.1163
7	-439.7472	0.0108

Table. S5 Detailed migration energy barrier of Zn^{2+} in V_2O_5-BQ4F model.

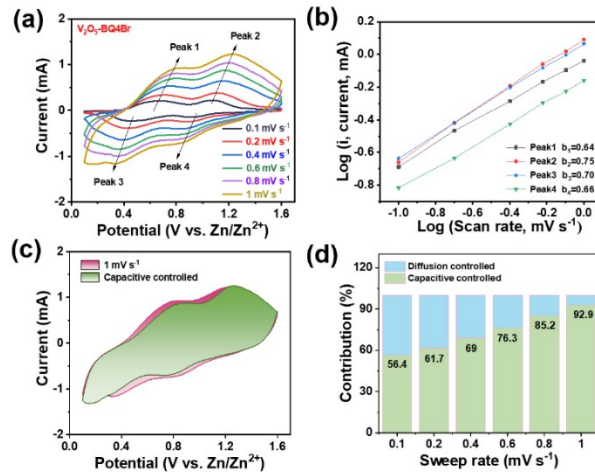| position	Etot/eV	Energy barriers/eV
1	-439.7816	0
2	-439.7404	0.0412
3	-439.3334	0.4482
4	-439.7502	0.0314
5	-439.7195	0.0621
6	-439.7064	0.0726
7	-439.939	-0.1574

Fig. S16 (a) CV curves at different sweep rates from 0.1 to 1.0 mV s^{-1} (b) Log (i) versus log (v) plots related to CV curves. (c) Capacitive contributions at 1 mV s^{-1} (d) the proportion of capacitive contribution from 0.1 to 1.0 mV s^{-1} of V_2O_5-BQ4Br.

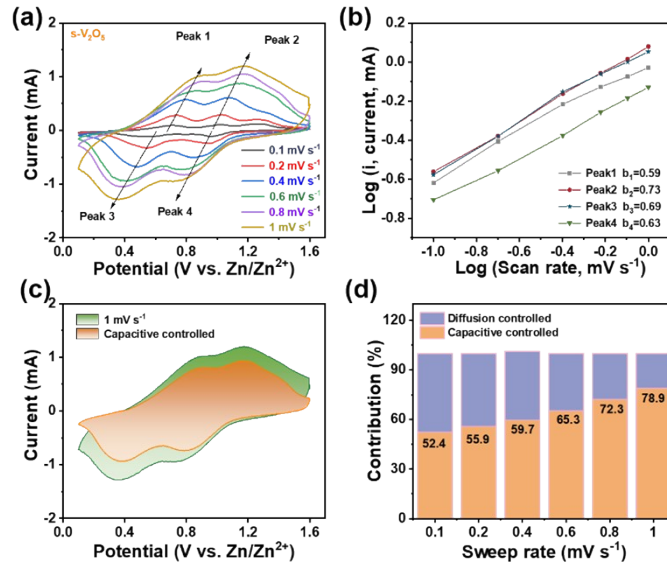**Fig. S17** (a) CV curves at different sweep rates from 0.1 to 1.0 mV s^{-1} (b) Log (i) versus log (v) plots related to CV curves. (c) Capacitive contributions at 1 mV s^{-1} (d) the proportion of capacitive contribution from 0.1 to 1.0 mV s^{-1} of s-V_2O_5.
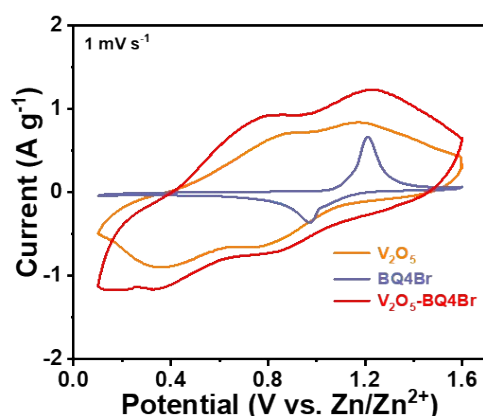
Fig. S18 CV curves at 1 mV s⁻¹ of V₂O₅, BQ4Br and V₂O₅-BQ4Br.

References:

1. G. Kresse, J. Furthmüller, *Mater. Sci.,* 1996, 6, 15−50.
2. G. Kresse, J. Furthmüller, *Phys. Rev. B,* 1996, 54, 11169−11186.
3. J. P. Perdew, K. Burke, M. Ernzerhof, *Phys. Rev. Lett.,* 1996, 77, 3865−3868.
4. G. Kresse, D. Joubert, *Phys. Rev. B,* 1999, 59, 1758-1775.
5. P. E. Blöchl, *Phys. Rev. B,* 1994, 50, 17953-17979.
6. S. Grimme, J. Antony, S. Ehrlich, and S. Krieg, J. *Chem. Phys*., 2010, 132, 154104.
7. S. Grimme, S. Ehrlich, L. Goerigk and J. Comp, *Chem*., 2011, 32, 1456.
8. P Hu, M Yan, T Zhu, X Wang, X Wei, J Li, L Zhou, Z Li, L Chen and L Mai, *ACS Appl. Mater. Interfaces,* 2017, 9, 42717-42722.
9. S Chen, K Li, K Hu and J Zhang. *Adv. Funct. Mater.,* 2020, 30, 2003890.
10. Z. Feng, J. Sun, Y. Liu, H. Jiang, M. Cui, T. Hu and Y. Zhang, *ACS Appl. Mater. Interfaces,* 2021, 13, 61154-61165.
11. K. Li, Y. Gong and J. H. Lin, *Chem. Eng. J.*, 2023, 452, 139621.
12. B. Wang, S. Dai, Z. Zhu, L. Hu, Z. Su, Y. Jin and L. Huang, *Nanoscale*, 2022, 14, 12013-12021.
13. Y Du, X Wang, J Man and J Sun. *Mater Lett.* 2020, 272, 127813.
14. X Liang, L Yan, W Li, Y Bai, C Zhu, Y Qiang, B Xiong, B Xiang and X Zou. *Nano Energy.* 2021.106164.
15. J. Zhang, S. Liu, S. Zhou, H. Liu, R. Ding, S. Wei and X. Lu, *ACS Sustain. Chem. Eng.*, 2022, 10, 10243-10251.